Fault Signature of a Flux-switching DC-field Generator

Fei Lin, K. T. Chau, *Fellow, IEEE*, Christopher H. T. Lee, and Chunhua Liu
Department of Electrical and Electronic Engineering, The University of Hong Kong, Hong Kong, China

Flux-switching DC-field (FSDC) machine has the merits of flexible flux control and low-cost. Furthermore, this type of machines also possesses the advantage of fault-tolerant capability. However, few of the research have been done on the analyses of fault signatures for this type of machines even though it has two sets of windings. This paper investigates the fault signature of a magnetless FSDC generator for its armature winding faults. It focuses on the study of short circuit (SC) faults and open circuit (OC) faults. For the SC fault cases, the prototyped machine is tested with one-phase half-turn SC fault and two-phase half-turn SC fault. For the OC fault cases, one-phase OC fault is investigated. The rectified output current is utilized as the fault indicator. Both simulation and experiment results are studied for the verification.

***Index Terms*—Fault signature, flux-switching machine, DC-field generator, short circuit fault, open circuit fault.**

I. Introduction

FLUX-SWITCHING DC-field (FSDC) machine has received a great interest in industrial applications [1]. Compared with the conventional permanent-magnet machine, it offers definite advantages of effective flux control and low-cost [2]. Owing to the adoption of both DC-field winding and armature windings on the stator, it is vulnerable to the stator winding faults, such as abnormal connection of windings, open circuit fault of windings, and short circuit fault of windings [3]-[5]. Hence, this feature of multiple sets of windings on the stator brings the machine an advantage of fault-tolerant capability [6]. However, in literature, none of the research has been done on the investigation of fault signatures of the FSDC machines.

The purpose of this paper is to investigate the fault signatures of a magnetless FSDC generator with armature windings faults, namely, the short circuit (SC) fault and open circuit (OC) fault. The rectified output current is used as fault indicator. The motor current signature analysis (MCSA) with Fast Fourier Transform (FFT) is carried out for the fault signature analysis. Hence, by conducting both experiment and simulation, these two fault signatures are detected, analyzed, and compared in this study for verification.

II. Fault Signature Analysis

Fig. 1 shows the configuration of a wind power generation system, which introduces the operation mode of the proposed FSDC generator [7]. It consists of the proposed FSDC generator with a built-in rectifier, a wind turbine with gearbox, a controller, and an inverter connecting to the grid. It can be noted that the system controllers capture the generator output voltage and current from the proposed FSDC generator. By comparing the generator output voltage and current with the set references of the controllers, it aims to achieve the efficient electric power transmission. Since the proposed FSDC is connected with a built-in rectifier, instead of the three-phase AC voltages and three-phase AC currents, the generator output current and voltage are more often monitored by the electric power system controllers practically [6]. Hence, this paper selects the rectified output current as the fault indicator.

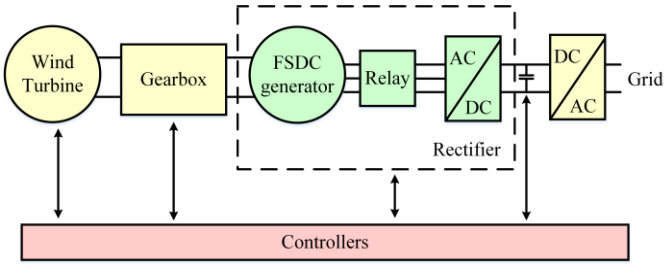

Fig. 1. Schematic diagram of a wind power generation system

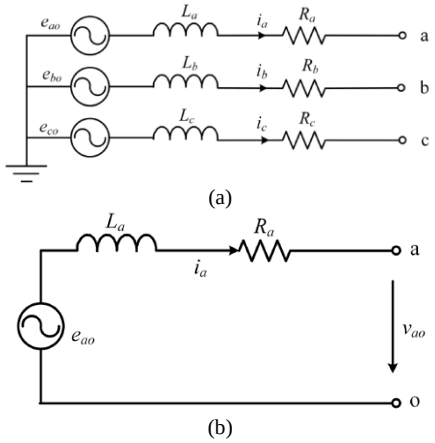

Fig. 2. Circuit representations of the proposed FSDC generator. (a) Three-phase circuit. (b) Simplified equivalent circuit of one phase

As shown in Fig. 2(a), e_{ao}, e_{bo}, and e_{co} represent the no-load electromotive forces (EMFs) of each phase, respectively. L_a, L_b, and L_c are the aggregated inductances of each phase, respectively. i_a, i_b, and i_c are the currents of each phase, respectively, and R_a, R_b, and R_c are the resistances of each phase, respectively. The circuit representation of each phase can also be simplified as indicated in Fig. 2(b). Hence, the relationship between the no-load EMF e_{ao} and the line-to-line voltage v_{ab} can be expressed as:

$$v_{ab} = e_{ao} - \left(L_a\, di_a/dt + R_a i_a\right) = N d\phi_a/dt - R_a i_a \qquad (1)$$

where N is the number of turns of phase A, Φ_a the magnetic flux linkage of phase A. It indicates the line-to-line voltage v_{ab} can also be expressed in terms of its flux linkage Φ_a [8].

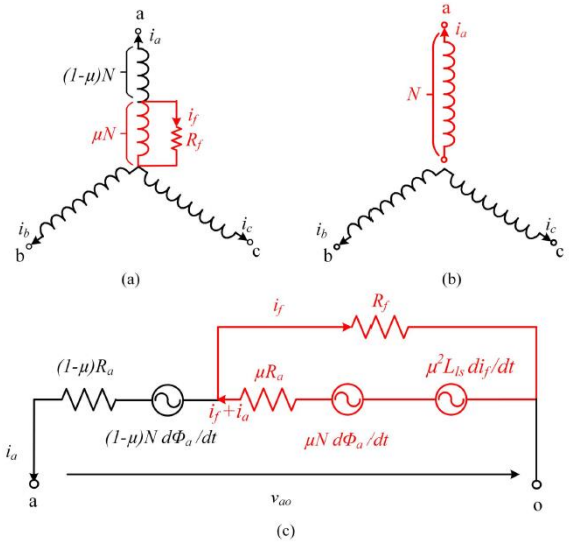

Fig. 3. (a) Three-phase representation of short circuit fault in phase A. (b) Three-phase representation of open circuit (OC) fault in phase A. (c) Phase A circuit representation under short circuit (SC) fault.

A. Short circuit (SC) fault

As shown in Fig. 3(a), N is the number of turns of each phase, R_f is the short circuit resistance, i_f is the short circuit current flowing into the short circuit resistance. Hence the current flowing into the shorted winding is (i_f +i_a). Assume the shorted part of phase A is determined by the coefficient μ (0-100%), hence μN represents the shorted part of phase A. The corresponding circuit diagram of phase A with short circuit fault is shown in Fig. 3(c). Hence, the line-to-line voltage v_{ab} can be expressed as:

$$v_{ab} = \left((1-\mu)Nd\Phi_a/dt - (1-\mu)R_a i_a\right) + \left(\mu Nd\Phi_a/dt - \mu R_a\left(i_a + i_f\right) - \mu^2 L_{ls} di_f/dt\right) \quad (2)$$

where $\mu^2 L_{ls}$ stands for the leakage inductance of the shorted turns. The fault current i_f in the shorted path can be given as:

$$R_f i_f = \mu Nd\Phi_a/dt - \mu R_a\left(i_a + i_f\right) - \mu^2 L_{ls} di_f/dt \quad (3)$$

By substituting (3) into (2), the relationship between v_{ab} and i_f can be deduced as:

$$v_{ab} = (1-\mu)R_a i_f + \mu(1-\mu)L_{ls} di_f/dt + R_f i_f/\mu \quad (4)$$

B. Open circuit (OC) fault

As shown in Fig. 3(b), since the entire phase is disabled, it becomes imbalanced with only two healthy phases under operation. The relationship between the average value of the rectified output current I_R and the first harmonic of phase current I under normal and one-phase OC conditions are given by (5) and (6) respectively:

$$I = 2\sqrt{3}/\pi I_R \approx 1.1 I_R \quad (5)$$

$$I = \sqrt{3}/2\pi I_R \approx 0.28 I_R \quad (6)$$

III. Implementation and Simulation

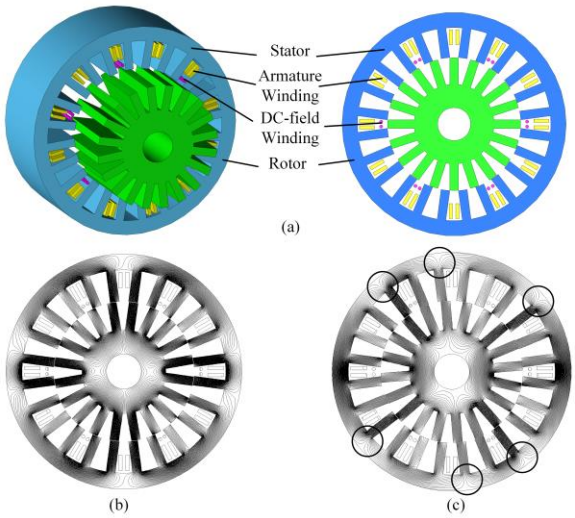

Fig. 4. (a) Exploded diagram of the proposed machine. (b) Magnetic field distribution under normal operation. (c) Magnetic field distribution under one-phase half-turn SC operation

By applying time-stepping finite element method (TS-FEM), performances of the proposed FSDC machine are presented. In the simulation, it investigates the magnetic field distribution and the rectified output current of the proposed machine under normal and faulty conditions.

First, Fig. 4(a) shows the exploded diagram of the proposed generator, which consists of the outer-rotor, the stator, the DC-field winding, and the armature winding. Second, the magnetic field distribution of the proposed machine under normal condition and one-phase half-turn SC fault of phase are showed in Fig. 4(b) and Fig. 4(c) respectively. It can be found that the flux lines are evenly and symmetrically distributed under normal operation. While it turns out to be asymmetrical under faulty operation. Especially in the circled areas, it can be observed that the flux line pattern of each stator pole become different due to the imbalance among the three phases. Fig. 5 is the three-phase current waveforms of the generator with load, which are sinusoidal with 120° conduction angles. Third, to discover the impact of stator winding faults on the performance, the rectified output current is investigated for both SC fault and OC fault. Fig. 6 is the comparison of the simulated rectified output currents under normal, one-phase half-turn SC fault, one-phase OC fault, respectively. When the generator is healthy, it can be found in Fig. 6(a) that all the rectified output current ripples have the same magnitude periodically. When the generator has half-phase SC fault in Fig. 6(b), the ripples become irregular. But it should be noted that a clear repetitive pattern of three current ripples appears. And the period of this pattern is three times of the period of the healthy one. When the generator has one-phase OC fault in Fig. 6(c), it is obvious that the three-phase windings become

imbalanced. Thus, the amplitude of the current ripple decreases significantly by comparing with the other two cases.

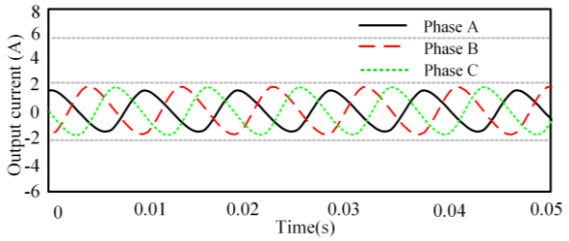

Fig. 5. Three phase current waveforms of the generator with load

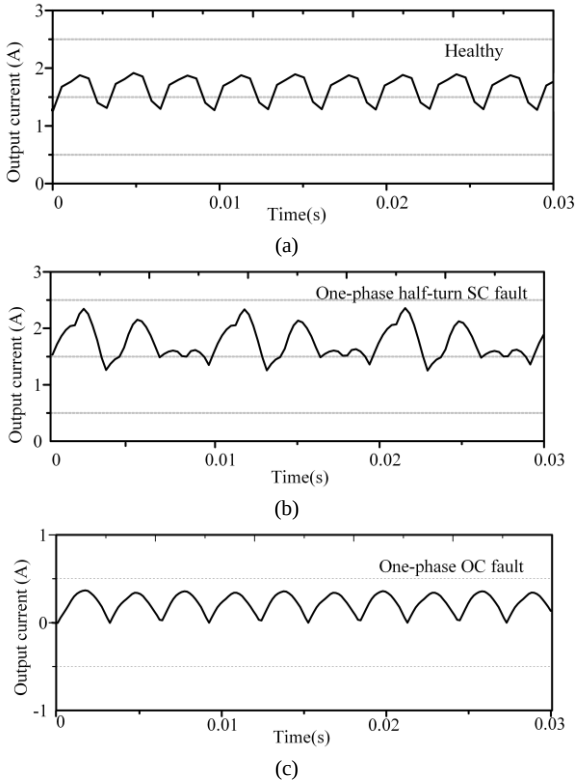

Fig. 6. Comparison of the simulated generator rectified output current under different conditions. (a) Normal. (b) One-phase half-turn SC fault. (c) One-phase OC fault.

IV. Experimental Validation

A three-phase FSDC generator is prototyped and experimented to verify the impact of SC fault and OC fault on the current. The experimental setup of the proposed generation system is established and as showed in Fig. 7, which consists of a dynamometer, a FSDC generator. The dynamometer acts to drive the FSDC generator. The FSDC generator is utilized to perform the fault analysis, where its armature winding connection can be rearranged for the faulty conditions. Since the FSDC generator is favorable for low-speed situation, the prototyped generator is driven by a dynamometer with the set speed of 300 r/min. For the purpose of comparison, the same stator winding faults that have simulated in the model are also tested and measured in the experiment.

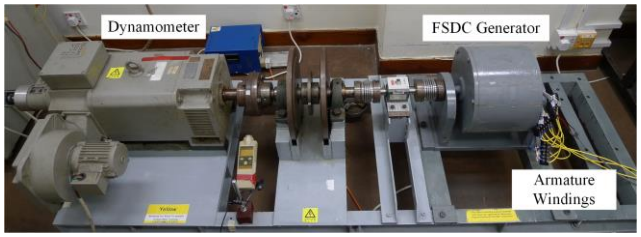

Fig. 7. Experiment setup for the proposed FSDC machine

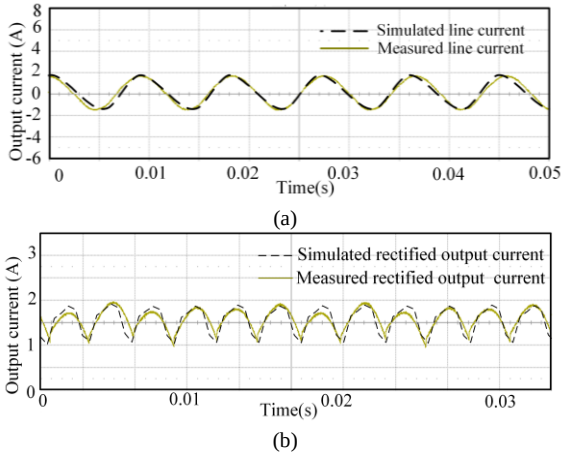

Fig. 8. Comparison of simulated and measured results under normal operation. (a) Phase A line currents. (b) Rectified output currents.

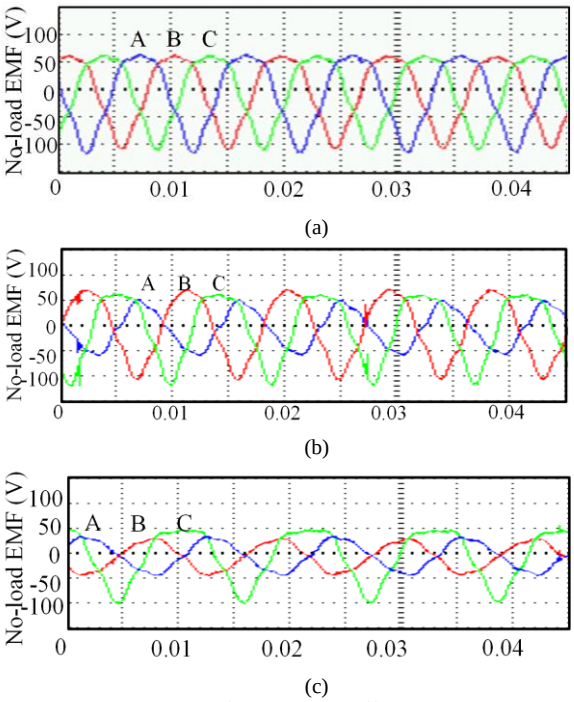

Fig. 9. No-load EMF waveforms under different conditions. (a) Normal operation. (b) Phase A half-turn SC fault. (c) Phase A & C half-turn SC fault.

Fig. 8 compares the normal line currents and rectified output currents by simulation and experiment respectively. Since the proposed FSDC generator is running at a rotating speed of 300 r/min, it has the period of 0.01s. As observed, the simulated currents agree very closely with the measured ones, which illustrates that the proposed model can accurately simulate the behavior of the faulty FSDC generator.

Fig. 9 shows the no-load EMF waveforms of the generator under different conditions. It is noted that the waveforms are not perfectly sinusoidal under normal condition in Fig. 9(a), which is due to the generator original design. In Fig. 9(b) and Fig. 9(c) under faulty conditions, it can be founded that the healthy phase keeps almost constant, while the faulty phases suffer from magnitude reduction, which results from the reduced internal resistance.

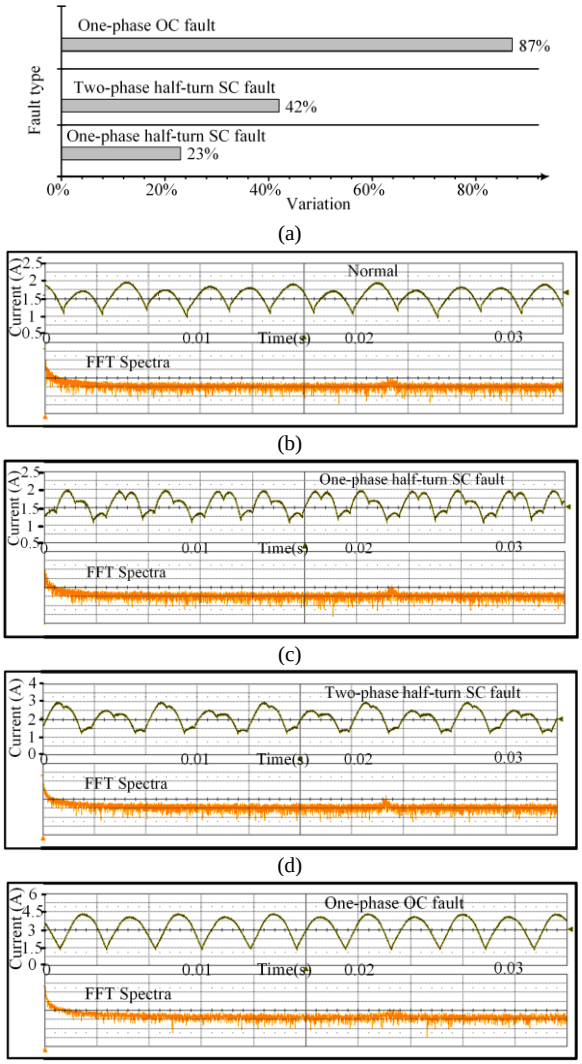

Fig. 10. Performances of the generator rectified output current and their corresponding FFT spectra (20 dB/div, 25 kHz/div). (a) Bar chart representation of the rectified output current variation under faulty conditions. (b) Normal. (c) One-phase half-turn SC fault. (d) Two-phase half-turn SC fault. (e) One-phase OC fault.

By verification, performances of the generator rectified output current of four types of conditions are presented in Fig. 10. Fig. 10(a) is a bar chart that summarizes the rectified output current variation in percentage. It is found that the one-phase OC fault has the most distinct variation of 87%, and the one-phase half-turn SC fault is the least one of 23%. The two-phase half-turn SC fault is the medium one of 42%. Their corresponding current waveforms are presented in Fig. 10(b), Fig. 10(c), and Fig. 10(d), respectively. As expected, the current ripples under faulty conditions are distinctly different from the one of the normal condition, which reveals in both magnitudes and periods of the repetitive pattern. The average output currents under normal, one-phase half-turn SC fault, two-phase half-turn SC fault, and one-phase OC are around 1.5A, 1.8A, 2.1A, and 3.0A respectively. It can be found that the variation of current is proportional to the reduced internal resistance. In addition, the corresponding spectra by FFT are also presented. It can be observed that the spectrum varies according to the distortion level of the current waveforms. The one-phase half-turn SC fault has the severe glitches, whereas the one-phase OC fault has the least glitches.

V. Conclusion

A FSDC generator is implemented in this paper for fault analysis since few of the research have been done on it. By verification, instead of the whole phase SC fault, half-turn SC fault and OC fault are tested and analyzed. In summary, it is illustrated that the simulated results agree fairly with the experimental result. And the OC fault has a more severe impact on the generator operation than the SC fault, which shows around 87% variation comparing to the normal operation. The one-phase half-turn SC fault shows the least variation of 23% by experiment, which proves the variation of the output current is proportional to the reduced internal resistance, and its spectrum varies from the distortion level of the current waveforms.

Acknowledgment

This work was supported in part by the Basic Research Program under Project JCYJ20120831142942515, in part by the Science, Technology and Innovation Commission of Shenzhen Municipality, China, and in part by the Research Grants Council, Hong Kong under Grant HKU 17200614.

References

[1] Y. Tang, J. J. H. Paulides, T. E. Motoasca, E. A. Lomonova, " Flux-Switching Machine With DC Excitation", IEEE Transaction on Magnetics, vol. 48, no. 11, pp. 3583-3586, Nov. 2012.

[2] C. Liu, K. T. Chau, J. Z. Jiang, "A Permanent-Magnet Hybrid Brushless Integrated Starter–Generator for Hybrid Electric Vehicles," *IEEE Transactions on Industrial Electronics*, vol. 57, no. 12, pp. 4055-4064, Dec. 2010.

[3] S. Nandi, H. A. Toliyat, and X.D. Li, "Condition monitoring and fault diagnosis of electrical motors-a review," *IEEE Transaction on Energy Conversion*, vol. 20, no. 4, pp. 719-729, Dec. 2005.

[4] C. Liu, K. T. Chau, and W. Li, "Comparison of fault-tolerant operations for permanent-magnet hybrid brushless motor drive," *IEEE Transactions on Magnetics*, vol. 46, no. 6, pp. 1378-1381, June 2010.

[5] B. Akin, S. B. Ozturk, H. A. Toliyat, and M. Rayner, "DSP-Based Sensorless Electric Motor Fault Diagnosis Tools for Electric and Hybrid Electric Vehicle Powertrain Applications," *IEEE Transaction on Vehicle Technology*, vol. 58, no. 5, pp. 2150-2159, June 2009.

[6] K. D. Hoang, Z. Zhu, M. Foster, "Direct torque control of permanent magnet brushless AC drive with single-phase open-circuit fault accounting for influence of inverter voltage drop," *IET Electric Power Applications*, vol. 7, no. 5, pp. 369-380, May 2013.

[7] C. H. T. Lee, K. T. Chau, C. Liu, D. Wu, S. Gao, "Quantitative Comparison and Analysis of Magnetless Machines With Reluctance Topologies," *IEEE Transactions on Magnetics*, vol. 49, no. 7, pp. 3969-3972, July 2013.

[8] Y. Tang, J. J. H. Paulides, T. E. Motoasca, E. A. Lomonova, " Energy Conversion in DC excited Flux-Switching Machines", IEEE Transaction on Magnetics, vol. 50, no. 11, pp. 1-4, Nov. 2014.